ANNUAL REPORT

FOR

NASA GRANT NAG-1-1063

PERIOD: JULY 1, 1991 - January 31, 1992

PRINCIPAL INVESTIGATOR:

BARRY T. SMITH

APPLIED SCIENCE PROGRAM
COLLEGE OF WILLIAM AND MARY
WILLIAMSBURG, VA 23185

NASA TECHNICAL OFFICER:

DR. PATRICK H. JOHNSTON

NONDESTRUCTIVE EVALUATION SCIENCES BRANCH
NASA, LANGLEY RESEARCH CENTER
MAIL STOP 231
HAMPTON, VA 23665

This annual report includes the work for the period of July 1, 1991 to January 31, 1992. The research for the first part of the grant period was reported in the semi-annual report for the period February 1, 1991 to June 30, 1991.

Included with this cover are the results for the work proposing the "Rapid Detection and Quantification of Impact Damage in Composite Structures". This article was presented at the American Helicopter Society Rotorcraft Structures Specialists' Meeting, Williamsburg, Virginia, October 1991. This article is included in the proceeding of the conference and we are submitting the article for publication in a refereed journal.

Rapid Detection and Quantification of Impact Damage in Composite Structures

Joseph N. Zalameda and Gary Farley
US Army Aerostructure Directorate AVSCOM
NASA, Langley Research Center Hampton, VA 23665

Barry T. Smith *
Applied Science
College of William and Mary
Williamsburg, VA 23185

* Work supported in part by NASA Grant NAG-1-1063.

INTRODUCTION

All new fixed and rotary winged military aircraft will make extensive use of composite materials to reduce weight and fabrication cost. These materials have been extensively used on secondary structure for more than a decade and are now beginning to be routinely used on primary structure. As the percentage of composite structure in an aircraft increases it becomes imperative to have reliable nondestructive inspection techniques to locate and quantify the extent of damage.

Composite materials exhibit significantly different damage/failure mechanisms than comparable metallic structures due to their laminated construction and generally weaker through-the-thickness mechanical properties. The issue of damage and failure mechanisms in a composite becomes more confusing with the inclusion of three-dimensional fiber architectures used to enhance damage tolerance. It is not uncommon for composite structures to exhibit invisible front surface damage from a foreign object impact but have extensive back surface damage.

Another potential damage/failure scenario with composite structure is related to disbonds between stiffeners and skin elements. Composite structures will make extensive use of cocuring or adhesive bonding of structural elements to eliminate the cost associated with mechanical fastening. Potential disbonds between elements can occur from manufacturing anomalies, excessive loads or as a result of foreign object damage. These disbonds are usually invisible and can not be detected or quantified except under precise laboratory conditions. Therefore, with the increased utilization of composites it is imperative to have reliable, accurate and rapid nondestructive evaluation (NDE) techniques to locate and quantify the damage and flaws.

There are many different NDE techniques used with composite materials and structure. These NDE techniques range from unsophisticated (tapping) to very high tech (CT scan). Considering the magnitude of the area to be inspected on an aircraft the process used to locate damage or flaw sites must be rapid. However, the NDE techniques that are applicable for quantizing damage are slow and can be only realistically applied to localized areas. Furthermore, the NDE technique should be one sided, that is the NDE technique should not require instrumentation located on both sides of the structure to perform the desired measurement. An approach to satisfy these requirements is to use two different one sided NDE methods thermography and ultrasonics. Thermography is used to rapidly locate the damage or flaw and ultrasonics is used to quantify the damage.

In this study NDE results from thermographic and volumetric ultrasonic techniques will be presented. Two types of specimens were used in this study, flat panels and a "Y" stiffened panel. Both types of specimens were fabricated from composite materials. Flat panels are fabricated with either carbon or Kevlar through-the-thickness (TTT) reinforcements. All specimens were impacted using an aluminum ball propelled by an air gun. Impact speed ranged from 91 to 167 m/sec. A brief discussion will also be presented on how the authors envision field deployment of thermographic and ultrasonic systems.

SPECIMENS

Two types of composite specimens were used in this study to demonstrate the effectiveness of thermographic and ultrasonic damage detection and quantification. They are integrally woven flat panels with TTT reinforcement, see Fig. 1, and a "Y" stiffener panel, see Fig. 2. These two different types of specimens are representative of the different material forms and structural complexity found on aircraft.

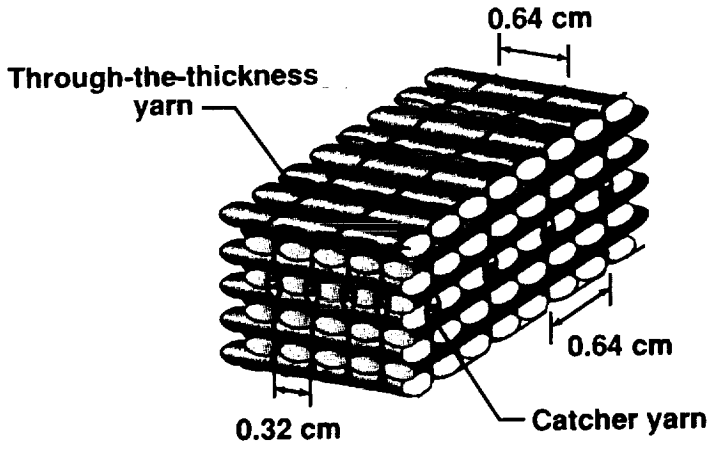

Figure 1: Integrally woven 3-D weave preform architecture.

The flat panels with TTT reinforcement were fabricated as dry integrally woven preforms. The TTT reinforcement was either Toray carbon stitching yarn or a 1100 denier Kevlar yarn. These panels had a fiber orientation of [0/90/0/90/0/90/0/90/0] composed of 21K filaments/yarn AS-4 carbon fibers. The 21K AS4 yarn was produced by combining 3K, 6K and 12K yarns. Row and column spacing of the TTT reinforcement was 0.64 cm creating a cell like grid. All preforms were infiltrated with 3501-6 epoxy resin and cured. The cured panels were approximately 0.64 cm thick. Three impact specimens of each TTT reinforcement type having dimensions 10.16 cm by 15.24 cm were machined from the cured panels (total of 6 specimens). The impact specimens were impacted with a 1.27 cm diameter aluminum ball using an air gun. One specimen of each TTT

reinforcement type was impacted with an energy of approximately 14, 27 and 41J.

The "Y" stiffened panel was 45.72 cm in length and 15.24 cm wide and having a stiffener width of approximately 10.16 cm, see Fig. 2. The skin of the panel was composed of 24 plies of tape prepreg

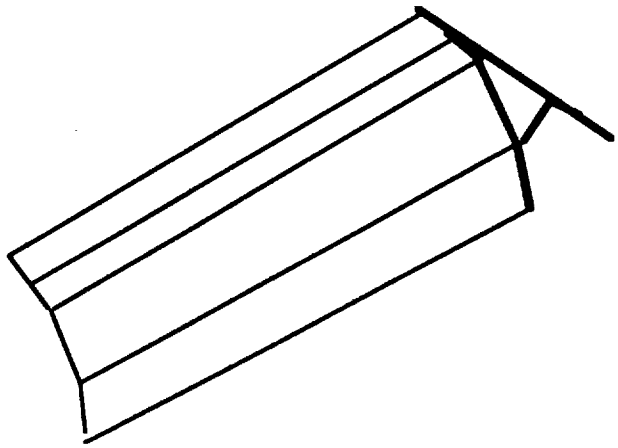

Figure 2: "Y" - stiffener panel.

having a stacking sequence of [(+45/-45/0)2 (-45/+45/90)]2S. The web of the stiffener was composed of 16 plies of tape prepreg having a stacking sequence of [(+45/-45/90)2/+45/-45]S. All prepreg material was IM7-8551-7 a high strain and rubber toughened system.

Aluminum ball impacts on the front surface (skin side) consisted of three along the stiffener flange and one mid-way between the stiffener flanges. Three impacts along the stiffener web and blade intersection on the stiffener side of the panel were made. The energy of the impacts were between 14 and 41J.

THERMOGRAPHY INSPECTION

The thermography technique has the advantage of being non-contacting single sided and able to examine fairly large areas rapidly. The impact damage was imaged by measuring differences in the sample's cool down response caused by thermal diffusivity changes. Thermal diffusivity is a material property governing the rate in

which heat flows within a material. An overview of the theoretical basis is presented followed by a description of the experimental method.

THEORETICAL BASIS

The thermal response of the composite was determined by assuming the composite was a single, homogeneous layer with flashed radiant heating at one surface (x = 0) and negligible convection losses. The derivation [1] for a normalized front surface temperature response follows. The one dimensional heat flow is described by the following equation:

$$\frac{\partial T(x, t)}{\partial t} = \alpha \frac{\partial^2 T(x, t)}{\partial x^2} \qquad (1)$$

with boundary conditions:

$$\frac{\partial T(x, t)}{\partial t} = \delta(t) \qquad \text{for } x = 0 \qquad (2),$$

and

$$\frac{\partial T(x, t)}{\partial t} = 0 \qquad \text{for } x = l \qquad (3),$$

where l is the layer thickness, α is the effective layer thermal diffusivity, and T(x,t) is the temperature. A solution for the temperature decay due to an impulse input at t = 0 to the front surface is given below as:

$$T(x,t) = \frac{Q}{2\sqrt{\pi \alpha t}} + \frac{Q}{2\sqrt{\pi \alpha t}} \sum_{n=1}^{\infty} \left(e^{-\frac{(x-2nl)^2}{4\alpha t}} + e^{-\frac{(x+2nl)^2}{4\alpha t}} \right). \qquad (4)$$

Where Q is the energy per unit area. The normalized cool down temperature response of the layer can be expressed from (4) as:

$$NT(0,t) = \sqrt{\frac{t_o}{t}} \left(1 + 2 \sum_{n=1}^{4} e^{-\frac{n^2 l^2}{\alpha t}}\right). \qquad (5)$$

where $t > to$, to is the time just after the heat impulse, and summing to the first four terms gives 6 place accuracy. Equation (5) is equivalent to normalizing with respect to the temperature immediately following the removal of heat. This normalization process helps to remove the uneven heating and surface emissivity variations.

For imaging it is convenient to define the averaged normalized cool down response for the layer front surface as:

$$\overline{NT}(0,t) = \frac{\sum_{t=t_o}^{t_f} NT(0,t)}{n}. \qquad (6)$$

This equation is plotted for different values of diffusivity in figure 3 with $t_0 = 1.0$ and $t_f = 93.0$ seconds. Discrete time steps of one second were used in the calculation. Impact damage tends to lower the diffusivity and therefore the lower normalized values would correspond to the damaged areas.

The time in which the heat diffuses through the material can be expressed in terms of the thermal time constant:

$$t = \frac{l^2}{\alpha}. \qquad (7)$$

Typically, lower layer diffusivity values require longer times for the heat to propagate into the sample. Any impedance mismatches (delaminations) will cause reflected energy to diffuse back to the surface thereby affecting the cool down response. The maximum inspection depth is dependent on such things as damage size and depth. Delamination diameters which are smaller than the depth are normally undetected [2].

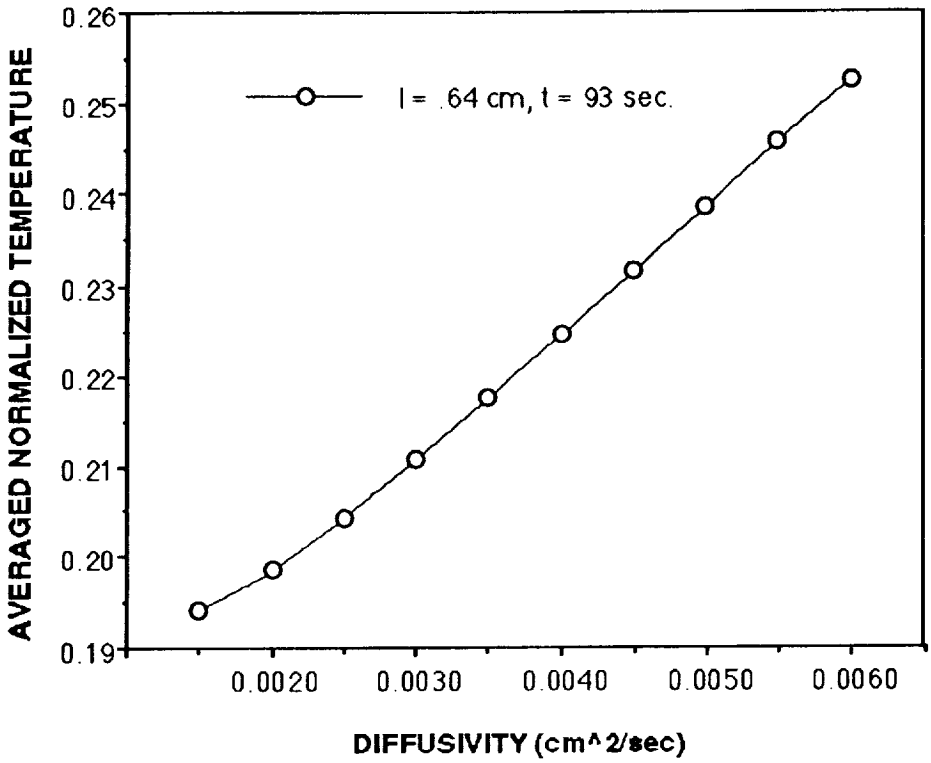

Figure 3: Variations in the cool down response due to diffusivity changes.

MEASUREMENT SETUP AND APPROACH

A typical thermal inspection system is shown in figure 4 and consists of four main components: the heat source, infrared camera, image processor, and computer. The heat source used in this study was commercially available photographic light sources. The light sources were Xenon flash tubes powered by a 6400 watt-second power supply. For symmetric heating two sources were used. The infrared camera was a scanned HgCdTe detector with a minimum temperature resolution of .1 degrees Celsius and a 2 milliradians instantaneous field of view. The camera output, 30 frames/sec., was connected to a real time image processor for digitizing, real time averaging, and storage. The computer controlled experimental parameters such as flash triggering, digitizing delay times and number of frames averaged. The computer was also used for subsequent data reduction.

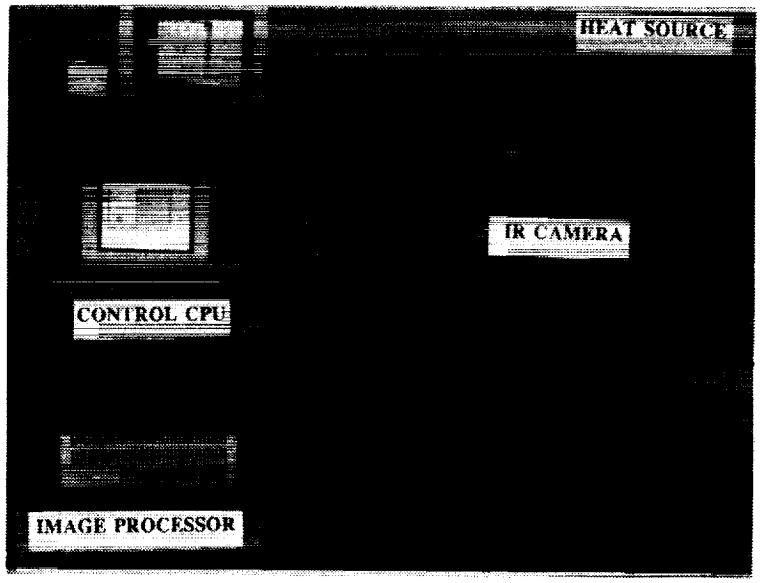

Figure 4: Thermal inspection setup.

The measurement protocol consisted of flashing the lamps to induce a thermal wave into the material. The video from the infrared camera was digitized and averaged in real time to capture the post heating images. A fixed number of averaged images (256 x 256 x 16 bits) were then stored within the image processor memory. The following equation was used to compute the output image:

$$\text{output image} = \sum_{n=j}^{k} \frac{(X_{i,n} - X_{i,k})}{(k - j) X_{i,j}} . \qquad (8)$$

Where i is the number of images averaged in real time per stored image, k is the total number of stored images, n is the stored image number (sequential in time from 0 to k), and j is the normalizing image number. Dividing by the image $X_{i,j}$ performed the normalization and subtracting image $X_{i,k}$ provided a background subtraction. The background subtraction was necessary to cancel out some fixed line distortion produced by the camera and also helped to reduce emissivity variations. The parameter i, number of images

averaged in real time, was calculated using equation (9). Equation (9) was derived from equation (7) by letting t = i/30 and l = $2l_d$. By adjusting i, the depth of inspection per stored image can be computed as:

$$l_d = \frac{\sqrt{\alpha\, i}}{10.95}. \qquad (9)$$

The TTT reinforced composite had 8 interfaces and therefore l_d was chosen to be approximately equal to the thickness of one interface. It is interesting to note that some through the thickness information is obtainable using this approach. By visually comparing respective output images for different values of j the best output image was chosen. The following values given in table 1 were used in the thermal inspections.

SAMPLE	TTT REINFORCED	Y - STIFFENED
*DIFF. (cm^2/sec.)	.0069	.0053
THICKNESS cm	.64	.34
AVE. FRAMES, i	90	128
STORED IMAGES, k	32	12
NORM. IMAGE #, j	3	0

TABLE 1: Measurement values used in the thermal inspections. *The diffusivity values were measured thermally using a technique discussed in reference [3].

ULTRASONIC INSPECTION

Ultrasonics is the most commonly used inspection technique for composites. Typical ultrasonic inspections consist of attenuation measurements over a given area using a through transmission configuration (C-scan). A C-scan measurement was made on the samples but a new method [4] also employed leads to increased detail

about the damage state of an impacted composite. The ultrasonic technique used in this study has the advantage of quantifying the defects by providing a volumetric through the thickness view. Using a pulse echo configuration, the total backscattered wave which includes the front, internal, and back surface reflections is used in the analysis. Signal processing and data visualization methods are used to provide impact damage images at different depths. An overview of the analysis is presented along with the measurement approach.

ANALYSIS

The material's response to an ultrasonic wave can be shown schematically as:

$$g(t) \rightarrow \boxed{h(t)} \rightarrow f(t) \qquad (10)$$

where g(t) is the input function, h(t) is the material transfer function and f(t) is the measured response. The functional relationship for a linear time invariant system is given by:

$$f(t)=\int h(t-t')\, g(t')\, dt'. \qquad (11)$$

The convolution of the input signal and material response leads to the measured output signal. To solve for the material's response equation (11) is evaluated in the frequency domain using Fourier transform techniques [5]. The Fourier transforms were all determined by numerical Fast Fourier Transform techniques. Thus the equation can be written for H(w), the material's response in the frequency domain, as:

$$H(w) = F(w) / G(w). \qquad (12)$$

G(w) was obtained by measuring the reflected signal off a brass plate. The impedance difference between brass and the composite was not used to renormalize the system response since we are only interested in relative differences between damaged and undamaged material. Taking the inverse Fourier transform of H(w) provides the deconvolved material response h(t) in the time domain. The complete deconvolved

result h(t) contains a solution for all frequencies up to the Nyquist limit. A suitable digital filter is used to window the results only over the bandpass of the transducer.

The output of the deconvolution procedure h(t) was used as the input to a calculation of the analytic function and finally its magnitude. The magnitude of the analytic function has been shown to be equal to the rate of arrival of the energy of the wave [6]. It should be noted that the energy measured was not corrected for phase cancellation effects at the face of the transducer. The form of the analytic function for the backscattered ultrasonic wave is determined by taking the Hilbert transform of the deconvolution h(t). This provides the imaginary part of the analytic function. The full complex analytic function can be written as:

$$h_A(t) = h(t) + i\, Hi[h(t)]. \qquad (13)$$

The complex part of (13) is the Hilbert transform of h(t) which is given as:

$$Hi[h(t)] = \frac{1}{\Pi}\int_{-\infty}^{\infty} \frac{h(t')dt'}{t - t'} \qquad (14)$$

The Hilbert transform is equivalent to the convolution of the signal with the kernel $1/(\pi t)$ and techniques for calculating the analytic function from the original signal are well documented [7]. Using complex Fourier transforms the material response in time space is Fourier transformed to frequency space where all the negative frequencies are zeroed before taking the inverse Fourier transform. This result is equivalent to the analytic form of the signal. The magnitude of the analytic function is then formed from the square root of the sum of the squares of the real and imaginary parts of the function. Applying this analysis gives the attenuation and depth information necessary for volumetric imaging.

MEASUREMENT APPROACH

The ultrasonic evaluation was performed in a water bath using a 5 MHz transducer with a 0.5 inch aperture and a 2 inch focal point for the woven samples. A 15 MHz transducer with a 0.125 inch aperture and a 2 inch focal length was used for the "Y" stiffener panel. The transducer was operated in a pulse-echo mode and was excited with a square wave pulser. The return signal was amplified and fed into a Time-Gain-Compensated (TGC) amplifier [8]. A digitizer with sampling rate of 50 or 100 MHz and 8 bit dynamic range acquired the signal and passed it to a computer for later analysis. The entire ultrasonic wave was digitized to include the front, interior, and back surface reflections. A spatial sampling step of 1 mm was on the order of the 3 dB point spread for the transducer as determined experimentally. A typical sampling size was 80x80.

The TGC has a 50 MHz bandwidth, a 50 dB gain, and a control bandwidth of 5 MHz. The TGC influence on the digitized signal is shown in Figure 5. The difference between the TGC on and off is quite dramatic. The front surface reflection is attenuated and the interior and back surface signals are enhanced to the input limit of the digitizer. This increases the effective dynamic range of the digitizer.

An example of the signal processed waveform using the analysis discussed previously is shown in figure 6. The front and back regions of the sample along with the ply interfaces are easily located.

RESULTS AND DISCUSSION

This section will present a comparison of the thermal images and ultrasonic "C" scan images. In addition, ultrasonic volumetric images showing damage at different ply interfaces will be shown.

DAMAGE DETECTION

The thermal and ultrasonic "C" scan images of the Kevlar and carbon TTT reinforced samples are displayed in figures 7 and 8 respectively. The top row are the thermal output images produced

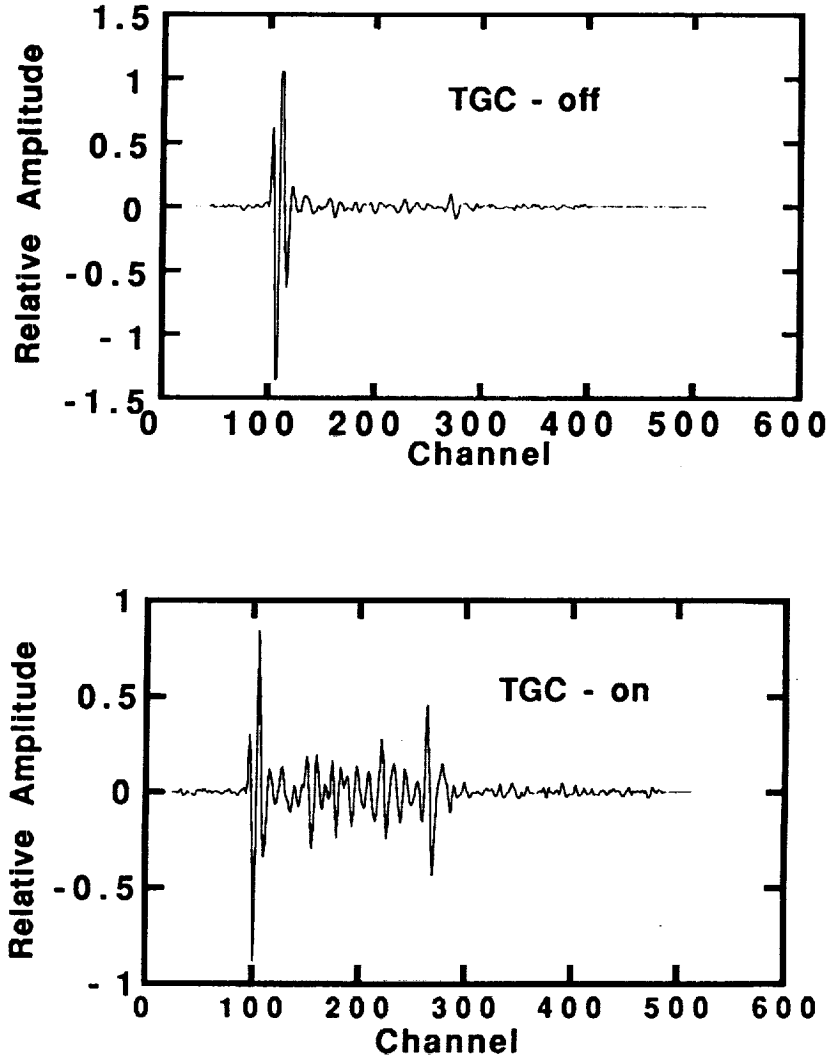

Figure 5. Waveform acquired with TGC off (top) and with TGC on.

using equation (8). The darker areas, which indicate the impact damage, represent longer times for the sample to cool down relative to the undamaged areas. The ultrasonic "C" scan images were produced by measuring the relative attenuation. The darker areas represent a greater attenuated signal thus indicating delaminations.

There seems to be an inconsistency for the 41J woven graphite sample. The thermal image reveals a smaller damage area than the

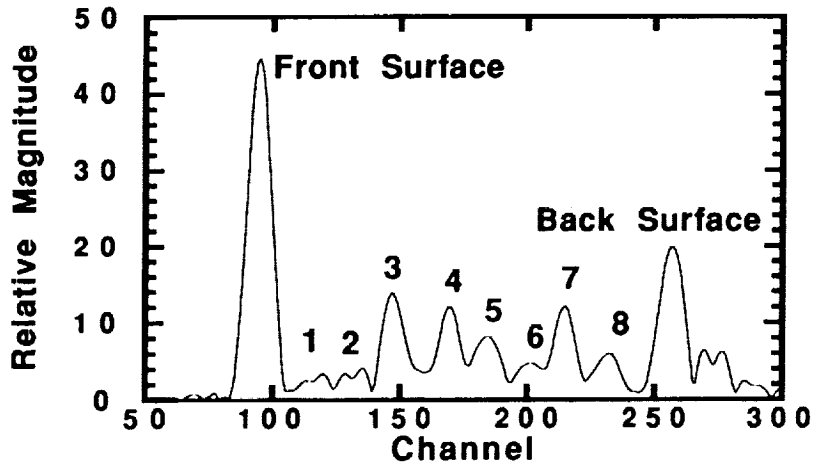

Figure 6. Result of deconvolution and analytic magnitude showing front and back surface, and 8 interfaces.

previous images at lower impact energies. The contrast for the 41J woven graphite sample is greater however, and by optimizing the grey map the resulting delamination area becomes larger. Implementing image enhancement techniques using a statistical histogram evaluation would be the next step in improving the thermal inspection.

The Y-stiffened top and side inspection images are shown in figures 9 and 10 respectively. The top view thermal image (middle image in figure 9) was not able to clearly define the smallest impact area. This was a result of the camera's limited resolution. The smallest impact area was detected successfully, however, by decreasing the camera's field of view. It is important to note the ultrasonic data for the side view (right image in figure 10) represents two separate scans one along the base of the stiffener (area A) and the other along the stiffener arm (area B). The side thermal image represents an angled view and therefore areas A, B, C, and D were all inspected at once. In addition to the side impact areas, the thermal image shows some flange damage in areas C and D due to the skin side impact.

The ultrasonic images provide more detail, but the inspection time is approximately an order of magnitude greater than the thermal

technique and also because thermal inspections are noncontacting complex geometries are more easily inspected. These advantages makes thermal an appropriate initial detection technique.

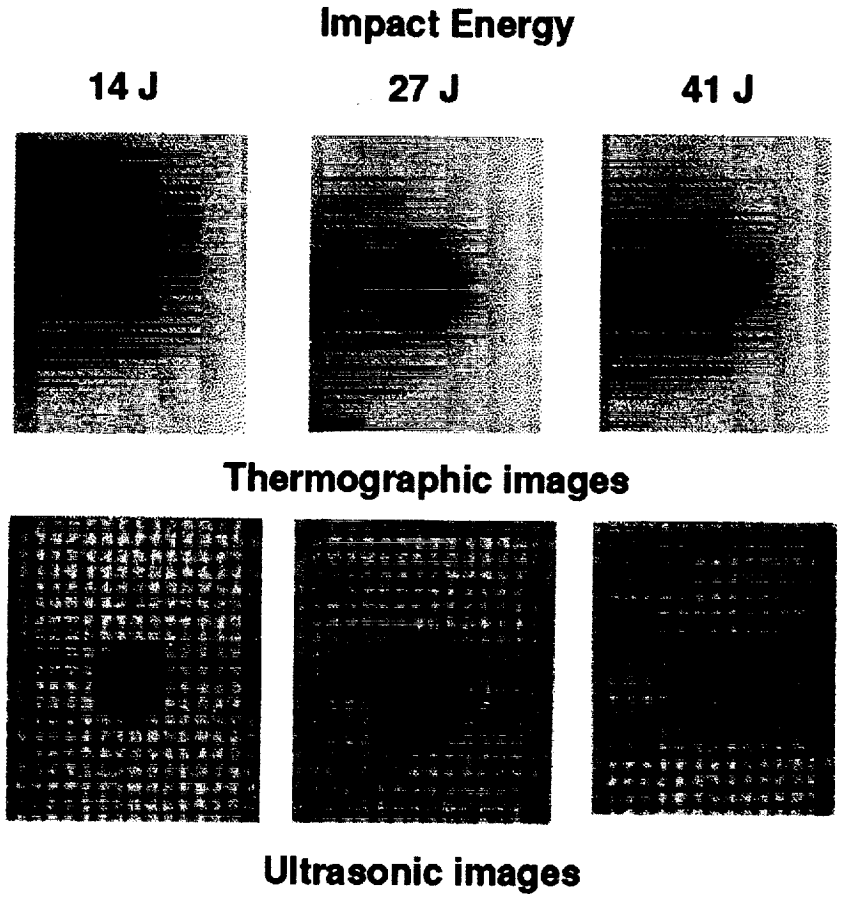

Figure 7: Thermal and ultrasonic "C" scan images of Kevlar TTT reinforced samples with damage produced from 14, 27, and 41 Joules energy impact.

DAMAGE QUANTIFICATION

The processed wave form shown in figure 6, clearly delineates the ply interfaces and the front and back surfaces. The location has

been localized in time over the original spread of the raw data and is a positive definite waveform. This data is arranged into a three

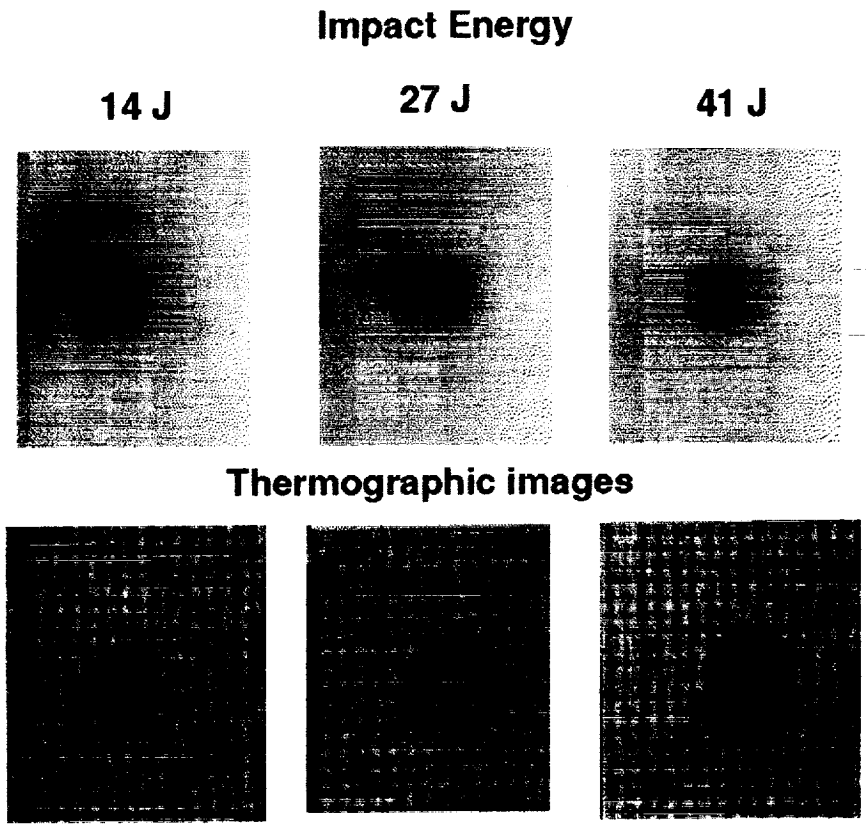

Figure 8: Thermal and ultrasonic "C" scan images of carbon TTT reinforced samples with damage produced from 14, 27, and 41 Joules energy impact.

dimensional array of x - y and time. The array can now be sliced in any of the three axis to compare the relative signal levels from any time and thus depth in the material. To view the damage from the impact side to the back surface the data is displayed on a computer

monitor sequentially in a movie type format. Each frame of the movie

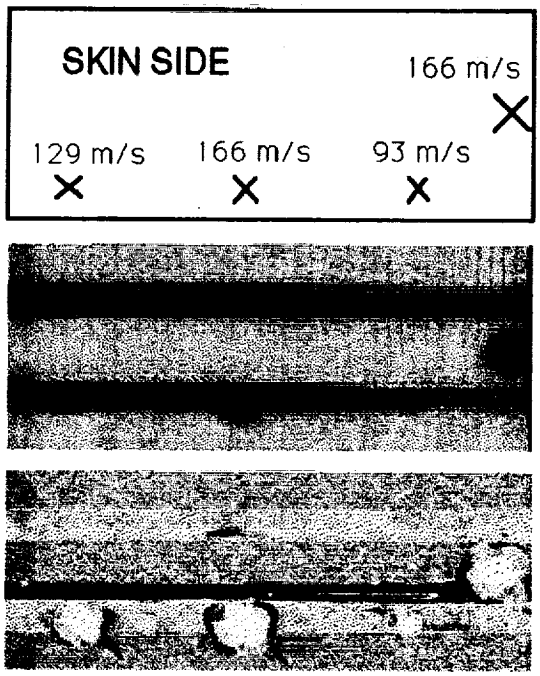

Figure 9: Inspection images of impact damage on the skinside of the Y- stiffened panel.

is a single digitized channel, and each frame is normalized to the 8 - bit dynamic range of the display. Since the digitized waveforms are in phase through the depth of the material, the relative backscatter at any depth is a measure of the impedance mismatch at that depth. In the case of a impact generated delamination, the relative amplitude is well above the average backscatter due to the ply interfaces. Using this method the damage at each interface can be clearly visualized.

A criterion for determining the total damage at each frame and thus depth can be identified. The area of the damage at each depth is much less than the entire frame area so that the image distribution is centered about the average background value of scatterers. The backscatter signal strength from the delaminations is well above this background level. A statistical analysis of each frame is a

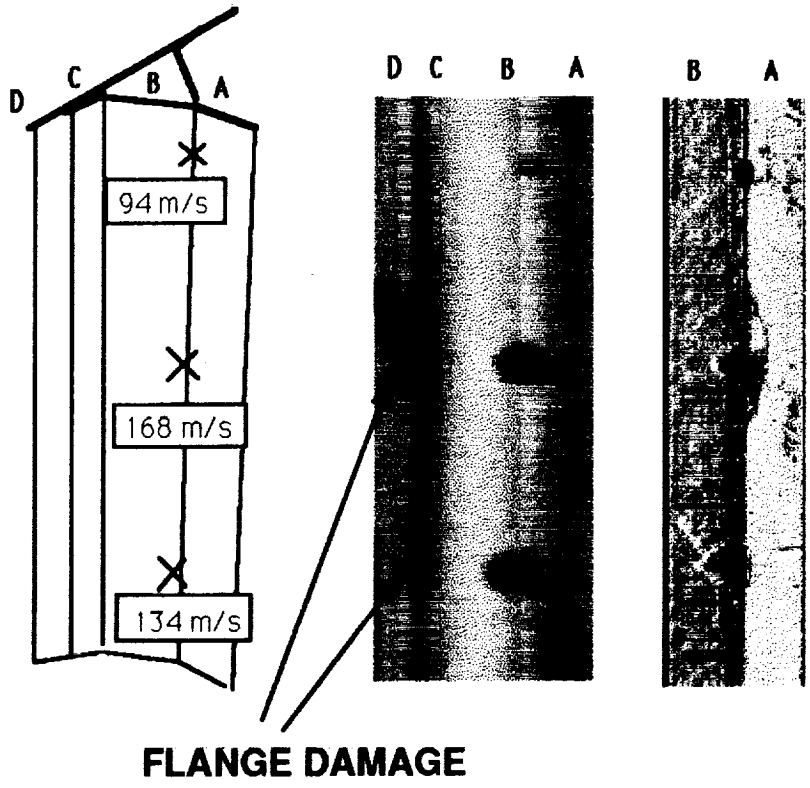

Figure 10: Inspection images of impact damage on stiffener side of the Y - stiffened panel.

means of determining the total area of damage. This was accomplished by calculating the standard deviation of the amplitude distribution of the entire 80x80 array for each frame in the movie. For the purpose of this analysis a standard 3σ greater than the median value (μ) of the distribution was taken as the lower limit for inclusion in the damage area. Thus for each frame every pixel value that was greater or equal to $\mu + 3\sigma$ was included in the damage area calculation for that frame.

Shown in figure 11 is the result of this calculation for the case of the carbon woven sample that had undergone a 41J impact. The numbers indicate the interlaminar location. The pixels that had

values greater than $\mu + 3\sigma$ are set at a white level and the rest of the pixels were left at their original gray level. The characteristic shape of the impact generated delaminations are well resolved. As the images move to the back surface the delamination areas are shadowed by the preceding delaminations.

A destructive test of the damage area is very difficult for these TTT reinforced samples. Sections were taken near the impact point, but visual determination of delamination cracks with a microscope at 100x were not possible. By soaking the sections in dye penetrant and taking an x-ray, some delamination cracks were visualized. The TTT reinforcements have the effect of keeping the cracks closed and it is felt the ultrasonic volumetric method gives a more realistic image of the impact generated delaminations.

The Y-spar section was imaged similarly for the volumetric damage and various interfaces are shown in figure 12. The scan size is 12 x 8 centimeters with a 0.1 cm step size. There are a possible 22 interfaces to image for the skin side of this specimen. All interfaces are detectable by a front surface ultrasonic volumetric method with some shadowing of underlying damage.

FIELD DEPLOYMENT OF THERMOGRAPHIC AND ULTRASONIC SYSTEMS

As previously shown the single sided thermographic system accurately detects the location of damage. The area that can be effectively scanned at a location is a function of the resolution of the thermographic camera, thickness of structure and heat transfer characteristics of the material. The scan rate to determine if any damage occurs or if a flaw exists is a function of CPU speed of the host microcomputer. With a current MAC microcomputer the entire process of acquiring and processing thermal data is on the order of a couple of minutes. This time decreases nearly linearly with computer CPU speed. The equipment used in this thermographic technique is very transportable.

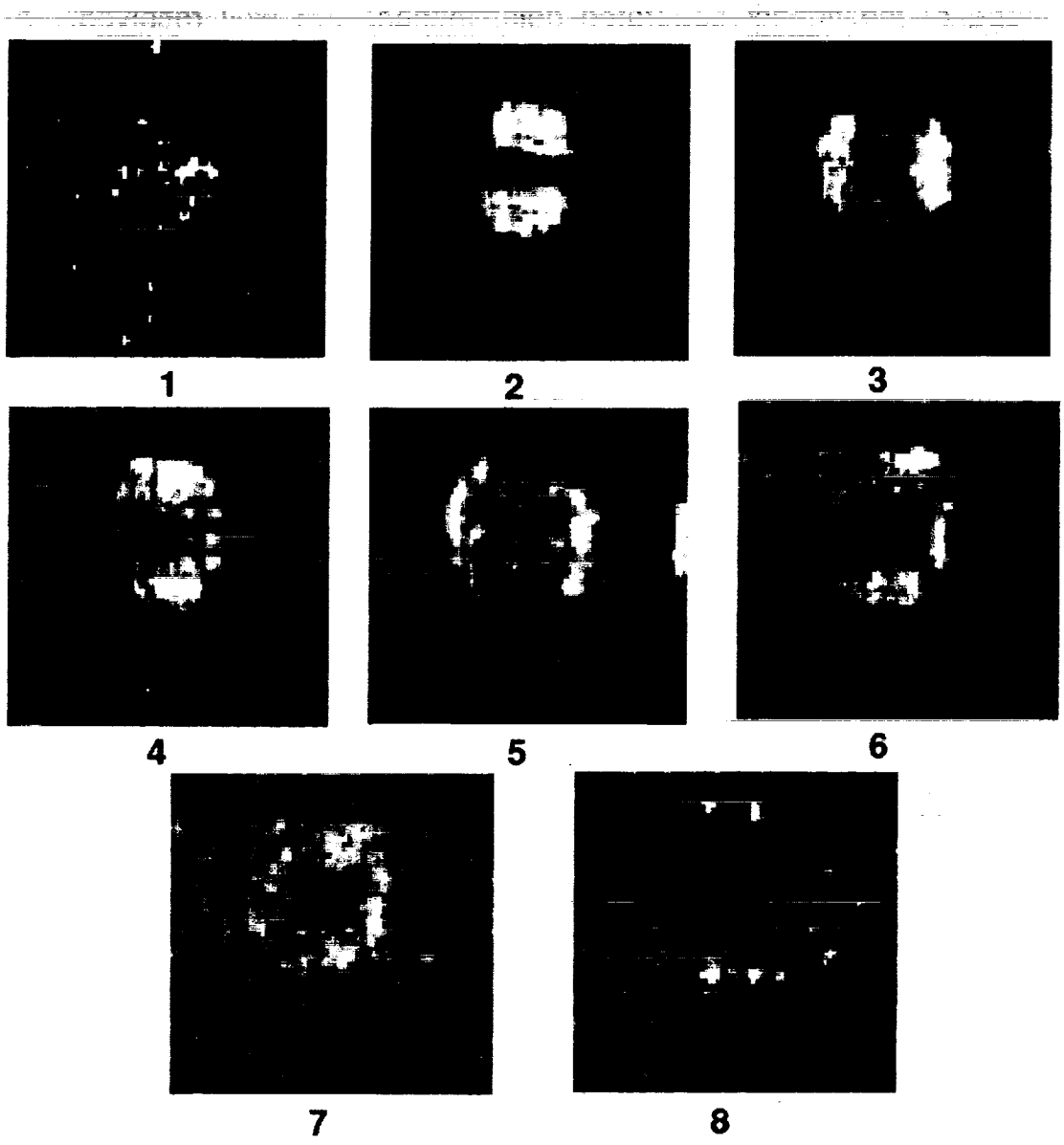

Figure 11: Through the thickness ultrasonic images for the carbon woven sample with 41J impact. Numbers indicate interlaminar location.

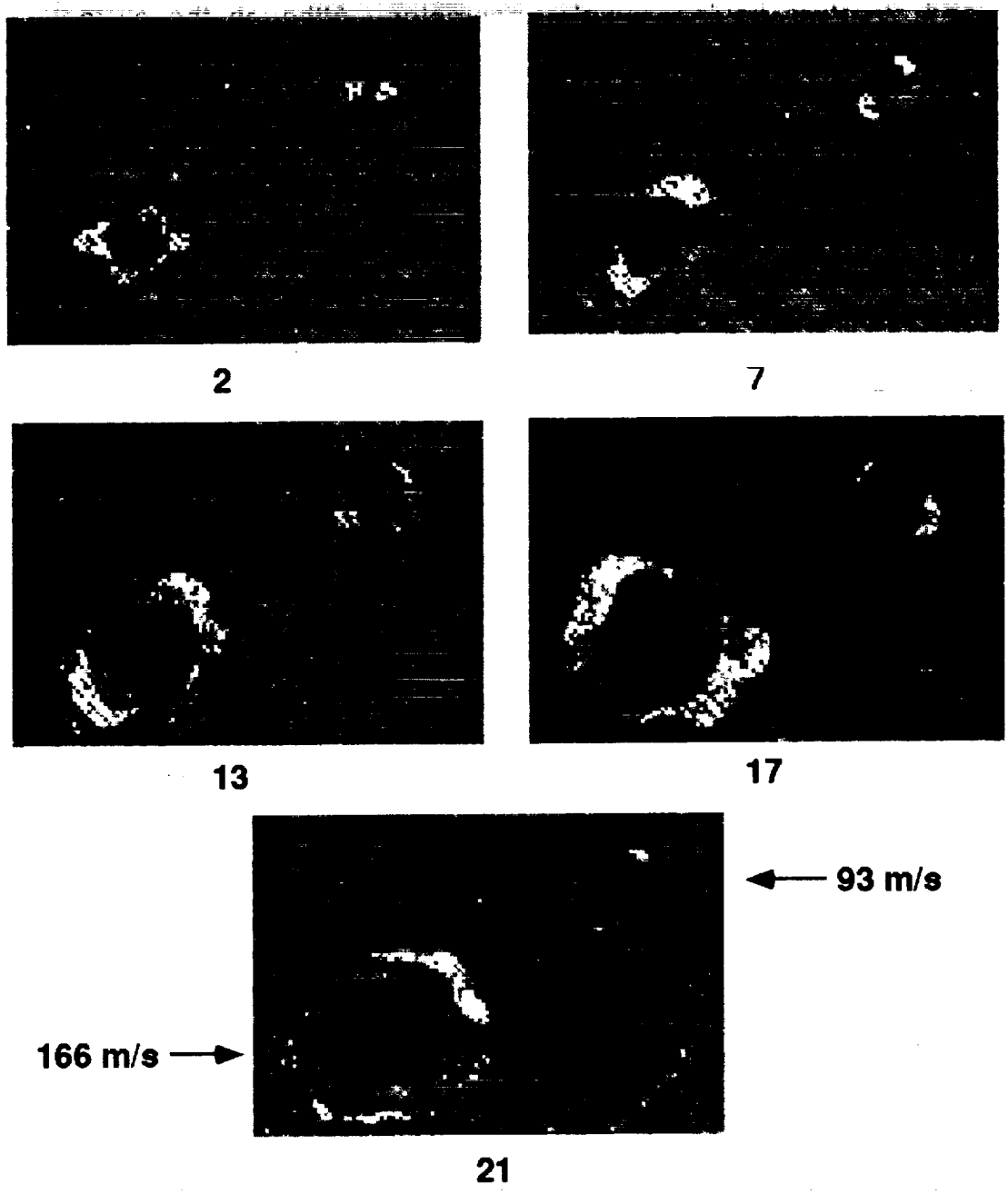

Figure 12: Through the thickness ultrasonic images of impact damage on the skin side of the "Y" stiffener panel. Numbers indicate interlaminar location.

Single sided volumetric ultrasonic imaging has been shown to provide details of internal damage in panels with TTT reinforcement and structure having complex geometry. Although the current investigation was conducted using a conventional water tank ultrasonic system, dry contact ultrasonic transducers are available. It is envisioned that a dry contact conformable array transducer can be fabricated to replace the water submersion system used in this study. The conformable array would be placed over the damage. Transducers in the conformable array would be scanned and an image of the internal damage would be produced.

A rendition of how the thermographic and ultrasonic systems can be field deployed is depicted in figures. 13 and 14. The heat source

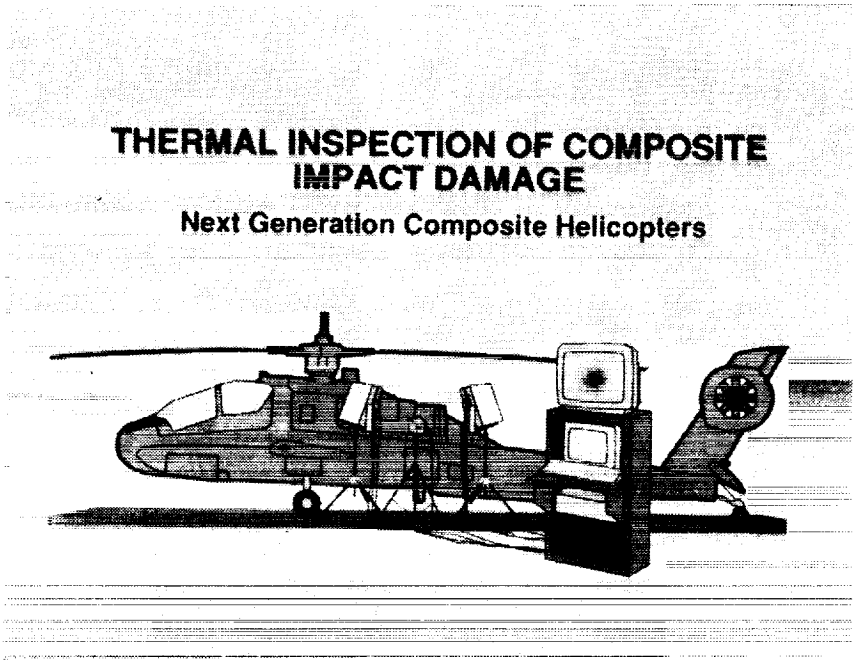

Figure 13: Field deployable thermographic inspection system.

lamps and thermographic camera are placed near the inspection location. The microcomputer and data acquisition system is contained in a console and can be moved along the aircraft. After a section of the helicopter is scanned for damage or flaws then the equipment is moved. When damage or a flaw is located then the spot is marked for ultrasonic inspection. A conformable dry contact array is place over the damage and the array is scanned. The data acquisition and data reduction console is position near the array and

a volumetric image of the damaged area is created. Data processing time is a linear function of computer CPU speed and generally requires only a few minutes on a RISC computer.

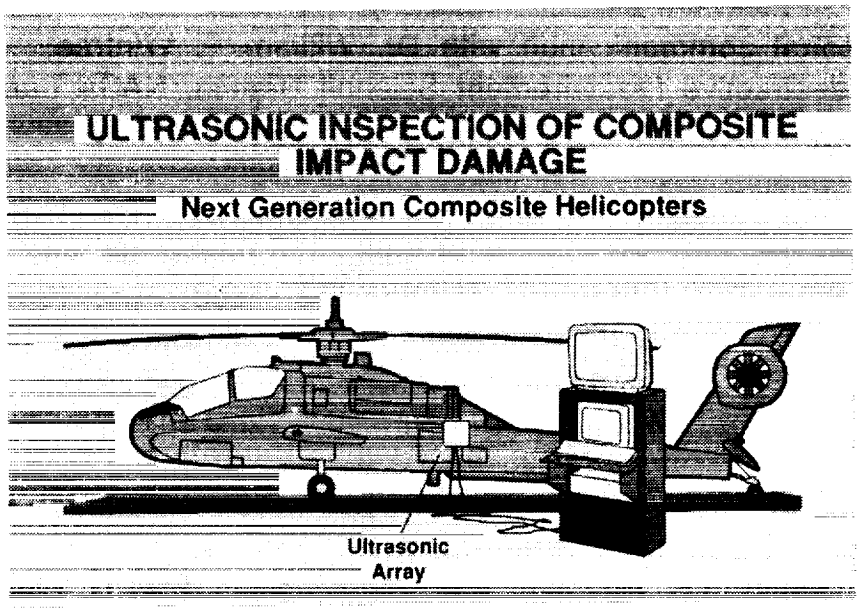

Figure 14: Field deployable ultrasonic imaging system.

CONCLUSIONS

This work demonstrates that a multidisciplinary NDE approach for impact damage detection in composite structures can be used to produce a more efficient inspection. The multidisciplinary NDE approach relies on fast large area thermographic inspections along with detailed ultrasonic volumetric imaging. The thermal inspection technique rapidly identifies the impact damage. The ultrasonic volumetric imaging quantifies the impact generated delaminations through the volume of the structure.

REFERENCES

1. Personal communication with Dr. William P. Winfree, Nondestructive Measurement Science Branch, NASA Langley Research Center, Hampton, VA, Oct. 1991.

2. P. Cielo, X. Maldague, A. Deom, and R. Lewak, "Thermographic Nondestructive Evaluation of Industrial Materials and Structures", Materials Evaluation, vol. 45, pp. 452 - 460, April 1987.

3. J. N. Zalameda and W. P. Winfree, "Thermal Diffusivity Measurements in Composite Porosity Samples", Review of Progress in Quantitative NDE, edited by D. O. Thompson and D. E. Chimenti (Plenum Press, NewYork, 1989), pp. 1541 - 1547, Vol. 9B.

4. B.T. Smith, J.S. Heyman, A.M. Buoncristiani, Earl D. Blodgett, J.G. Miller, and S.M. Freeman, Correlation of the Deply Technique with the Ultrasonic Imaging of Impact Damage in Graphite/Epoxy Composites, Materials Evaluation, vol. 47, No. 12, December 1989, pp1408-1416.

5. Bracewell, R.N. , *The Fourier Transform and Its Application*, McGraw-Hill, New York, (1982)

6. Heyser, R.C. ,"Determination of Loudspeaker Signal Arrival Times Part III", *Journal of the Audio Engineering Society*, vol. 19, pp 902-905, (1971).

7. Gammell, P.M. ,"Improved Ultrasonic Detection Using the Analytic Signal Magnitude", *Ultrasonics*, vol. 19, pp 73-76, (1981).

8. NASA Tech Briefs, June 1987, p. 28.